American Mineralogist, Volume 75, pages 723–730, 1990

Atomic structure and morphology of the albite {010} surface: An atomic-force microscope and electron diffraction study

MICHAEL F. HOCHELLA, JR.
Department of Geology, Stanford University, Stanford, California 94305, U.S.A.
CARRICK M. EGGLESTON
Department of Applied Earth Sciences, Stanford University, Stanford, California 94305, U.S.A.
VIRGIL B. ELINGS, MATTHEW S. THOMPSON
Digital Instruments, Inc., 6780 Cortona Drive, Santa Barbara, California 93117, U.S.A.

ABSTRACT

The atomic structure and nanometer-scale morphology of the {010} surface of albite, exposed by fracturing in air at room temperature, has been studied with low-energy electron diffraction (LEED) and contact atomic-force microscopy (AFM). The LEED results suggest that this surface is very similar to a simple termination of the bulk structure; however, there is evidence that the surface structure exhibits slight lateral relaxation owing to modest shifts of surface atoms as they seek equilibrium positions in this low symmetry structure. The AFM used in this study has demonstrated a lateral resolution as low as 1–10 nm depending on surface roughness (better lateral resolutions, in the range of 0.1–1 nm, are achievable) and a height resolution of 0.1 nm. Several reactive sites on the albite {010} surface have been imaged at this resolution, including very small pits and cleavage steps. These types of structure and morphological analyses on mineral surfaces have a direct application to studies dealing with mineral dissolution, sorption reactions on mineral surfaces, and fracture propagation.

INTRODUCTION

The field of mineral-surface geochemistry has grown dramatically because of its importance in environmental issues and its wide-reaching applications to the general field of water-rock interaction. It is becoming increasingly clear how surface reactions strongly influence the interaction of minerals with their surroundings and why bulk reactivity and thermodynamics often are not sufficient to fully explain observed geochemical phenomena. As a result, the study of the factors that control mineral surface reactions (surface atomic structure, composition, and morphology) has become a new subfield of mineralogy. Also very recently, scanning-tunneling and atomic-force microscopy and spectroscopy have revolutionized the field of surface science. These techniques have allowed workers in many surface-related disciplines to understand surface structure and reactivity as never before because they allow imaging of surfaces down to the atomic level, and, in certain cases, individual atoms and surface reaction sites can be identified.

The application of scanning-tunneling microscopy and spectroscopy to mineralogy has begun (Hochella et al., 1989; Eggleston and Hochella, 1990), although this work is restricted to conducting and semiconducting minerals (e.g., certain oxides and sulfides). In this paper, we introduce the use of contact atomic-force microscopy (AFM) and low-energy electron diffraction (LEED) to determine the morphology (down to the Ångstrom level) and the atomic structure of the surface of insulating minerals. For this particular study, we utilize these techniques to investigate the albite {010} cleavage surface. We have chosen albite because of its well-known bulk structure and chemistry, as well as its general mineralogic and geochemical importance.

AFM background

The atomic-force microscope was first introduced by Binnig et al. (1986) and has evolved to a considerable degree and taken on a number of interesting variations (see, e.g., Alexander et al., 1989, and references therein; Pool, 1990). AFM does not depend on tunneling current (as does tunneling microscopy and spectroscopy) and can be used on nearly any surface, either conducting or insulating. To date, the AFM has demonstrated atomic resolution on graphite (e.g., Binnig et al., 1987; Albrecht and Quate, 1988), boron nitride (e.g., Binnig et al., 1987; Albrecht and Quate, 1987), and amorphous SiO_2 (Marti et al., 1987; Heinzelmann et al., 1988; Alexander et al., 1989), as well as a few other insulating materials (e.g., Hansma et al., 1988, and references therein). In addition, Hartman et al. (1990) have obtained intriguing AFM images of the montmorillonite and illite {001} surfaces at nearly atomic resolution. AFM is also versatile in that it can be operated in a vacuum, in air, and in water (e.g.,

0003–004X/90/0708–0723$02.00

Marti et al., 1987; Weisenhorn et al., 1989; Drake et al., 1989). However, it should be noted that AFM is in an earlier stage of development than tunneling microscopy and the full potential of this instrument has not yet been realized.

The AFM used for this study (a commercial instrument built by Digital Instruments, Inc.) operates in the contact mode by rastering a sample under a tip, which makes physical contact with the sample surface (Fig. 1). The tip (in this case a diamond fragment no larger than a few micrometers in any dimension) is cemented to the end of a SiN microcantilever. The force between the tip and sample is measured by the bending or deflection of the cantilever. The diamond tip is brought in contact with a sample surface with an exceptionally small force in the range of 10^{-7} to 10^{-9} N, and the sample is rastered under the tip by means of a single-tube piezoelectric translator (Binnig and Smith, 1986). The vertical movement of the diamond as it rides over the sample surface is measured by a laser beam reflecting off the back side of the microcantilever into a photodiode position sensor. This arrangement provides an optical lever arm which is capable of detecting a vertical movement of the tip of less than 1 Å. Images are obtained by either (1) detecting and recording the vertical movement of the tip as the sample is moved laterally beneath it (variable deflection mode), or (2) keeping the tip stationary by rastering the sample in x, y, and z (constant force mode). In the latter case, a feedback loop is used to adjust the sample height in order to keep the reflected laser beam stationary within narrow limits with respect to the position sensor. This method is preferable when dealing with fragile surfaces.

The microcantilevers and piezoelectric translators are designed to have high resonant frequencies (between 10 and 100 kHz) to reduce their sensitivity to external vibrations and provide adequate stability for high resolution AFM. Therefore, only minimal vibration isolation is needed. Adequate isolation can be achieved, for example, by suspending a heavy microscope platform from elastic cords. Atomically flat surfaces, as measured with this microscope, have a relief of less than 0.1 nm, putting an upper limit on any noise contributions. The calibration of the lateral distances for the AFM images shown in this paper is performed by imaging diffraction gratings with known spacing.

LEED background

LEED has been a standard tool for surface crystallographers for some time (e.g., see Clarke, 1985, and Van Hove et al., 1986, for reviews), although the study of the surface crystallographic properties of minerals is just beginning (Hochella et al., 1989). LEED has definite similarities to three-dimensional X-ray and high-energy electron diffraction, but the scattering of low-energy electrons from condensed matter gives essentially two-dimensional information from the surface. At the energy of the electron beams used for LEED (usually between 50 and 200 eV), elastic backscattering is only possible from the upper few (4–6) atomic layers of a silicate (e.g., see Hochella and Carim, 1988, and Seah and Dench, 1979), forcing LEED diffraction patterns to exhibit essentially only the two-dimensional symmetry of the near-surface region. Symmetry constrained to two dimensions is considerably simpler than in the three-dimensional case, with only 5 two-dimensional lattices, 10 two-dimensional point groups, and 17 two-dimensional space groups (e.g., see Henry and Lonsdale, 1969). Using the methods outlined in Hochella et al. (1989), it is relatively straightforward to determine the surface unit-cell size and shape and either to uniquely determine or to limit the possibilities of the two-dimensional space-group symmetry of a surface. Solving a surface atomic structure requires intensity information and is considerably more difficult.

There is one potential problem with surface diffraction of insulating surfaces that deserves mention here. Whenever an electron beam impinges on an insulator, charging can occur. Even slight charging can cause disruption of the trajectories of low-energy electrons. In this case, a diffraction pattern cannot be obtained. Charging occurs when the number of electrons entering the sample (equal in this case to the flux of the primary electron beam) does not equal the number of electrons leaving. The outflux of electrons results from both elastic and inelastic backscattering of primary beam electrons and also by the ejection of electrons in the near-surface of the sample (secondary electrons). Fortunately, the primary beam energy has a strong effect on the probability of secondary electron ejection (e.g., see Hochella, 1988, and references therein), and often it can be adjusted so that the electron influx is the same as the outflux. Because of the nature of secondary electron emission as a function of primary beam voltage, there are two so-called crossover voltages where neutrality occurs (e.g., Dawson, 1966). For silicates, we have found that LEED can be performed at the low crossover voltage (generally between 50 and 150 eV), whereas Auger spectroscopy is performed at the high crossover voltage (generally between 2 and 3 keV; see Hochella et al., 1986).

Experimental

The AFM images shown in this paper were obtained using a SiN microcantilever approximately 100 μm long and 1 μm thick (supplied by Park Scientific) with a diamond chip cemented to its end (see above). These particular microcantilevers have a spring constant of approximately 1 N/m. All images were collected in ambient air with the AFM on a vibration isolation stand. The microscope was run in the constant-force mode with an estimated tracking force of no greater than 10^{-7} N. Although AFM tips probably have the potential to damage softer surfaces in this force range (Abraham and Batra, 1989), we saw no evidence of surface damage at the level of resolution of our albite images. All images shown in this paper were stable and reproducible.

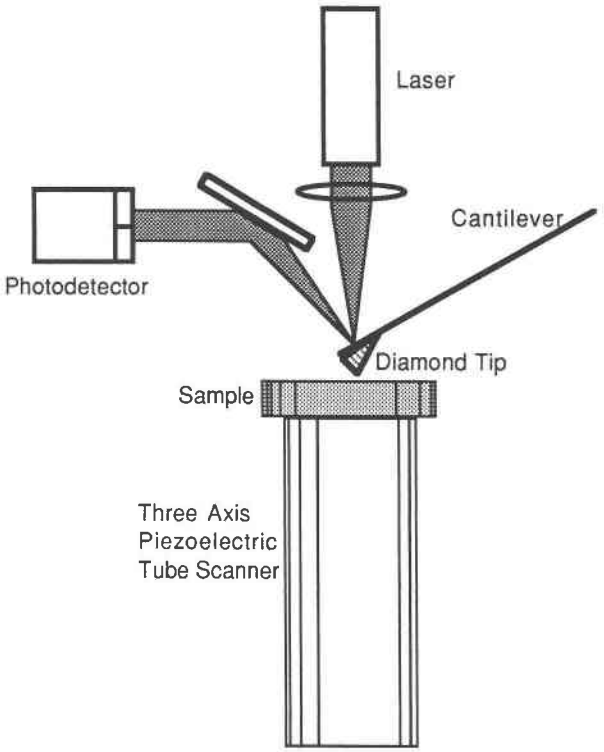

Fig. 1. Schematic drawing of an AFM showing the laser with lens (the latter not labeled), reflecting mirror (not labeled) and photodetector (photodiode position sensor), microcantilever with diamond tip attached, and a piezoelectric tube scanner, which moves the sample under the tip. This entire assembly is about 10 cm in height.

The LEED instrument used was a VG model 640-2 RVL reverse-view system mounted on a VG ESCALAB ultra-high vacuum chamber. The electron beam diameter at the sample surface is approximately 0.5 mm. Diffraction patterns of the albite {010} surface were taken with beam energies between 85 and 110 eV, and reciprocal distances were converted to direct distances according to the methods described by Hochella et al. (1989). The largest errors in the calculation of direct space distances come from the measurement of the diffracted beam spacings. LEED spots can be relatively diffuse, and there is some uncertainty in the scale change between the LEED fluorescent screen and its photographic reproduction. It is estimated that the uncertainty in calculated direct space distances using our LEED system is approximately $\pm 1\%$.

The albite samples used in this study, obtained from the Stanford Mineral Collection, are from pegmatites near Amelia, Amelia County, Virginia. This end-member albite shows excellent {010} cleavage. Large, milky white, single crystals were chosen that had no visible inclusions. The samples were cleaved in air (no other sample preparation was performed) and immediately analyzed with LEED or AFM. Specific surfaces chosen for study showed a mirrorlike flatness.

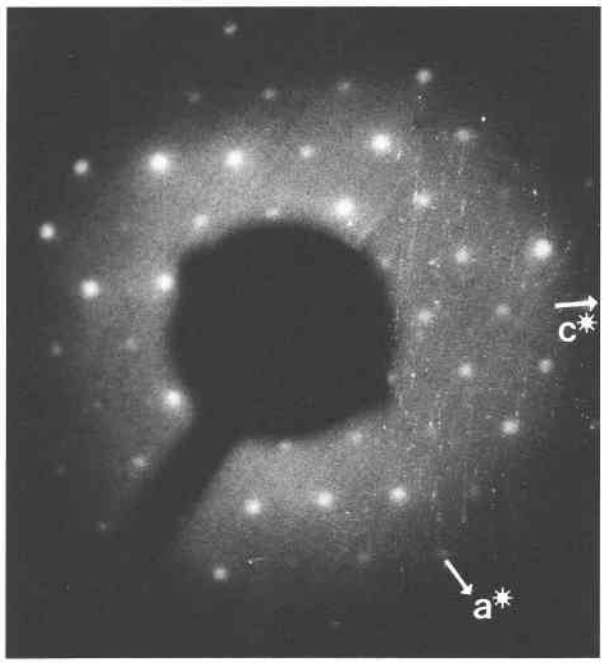

Fig. 2. A LEED pattern of the albite {010} cleavage surface showing the **a***-**c*** net. This pattern was collected at a primary beam energy of 87 eV. See text for details.

Results and discussion

LEED

A LEED pattern of the albite {010} surface, collected at 87-eV primary beam energy, is shown in Figure 2. This same pattern was consistently obtained over the entire exposed {010} surface of this and a second crystal. Measured repeat distances in this **a***-**c*** net are d(10) = 7.22 Å and d(01) = 6.51 Å, and β^* is 60°. Although d(10) is within the estimated error ($\pm 1\%$) of the expected value for bulk albite [d(100) = 7.28 Å], d(01) is nearly 2% higher than the bulk value [d(001) = 6.39 Å] and the measured β^* is well below the bulk value of 63.5°. The pattern has no systematic absences, and it is consistent with the oblique two-dimensional space group, $p1$.

It is interesting to compare this LEED pattern with single-crystal X-ray and electron diffraction of the **a***-**c*** net. Because of the usual choice of a nonprimitive unit cell for albite (for easier structural comparison with other feldspars), which results in the unconventional space group $C\bar{1}$, there is a systematic absence along **a*** ($h0l$, $h = 2n$). This absence is not seen in the LEED pattern, which can be explained by the two-dimensional nature of low energy diffraction. In the case of albite, the **c**-centering lattice point is halfway along **b** (which = 12.8 Å), meaning that it is several monolayers below the surface. It is this lattice point that causes the apparent absence along **a***. However, the LEED diffraction pattern, as stated earlier, results from diffraction from only the top 4–6 monolayers in silicates. In the case of Figure 2, this pattern probably

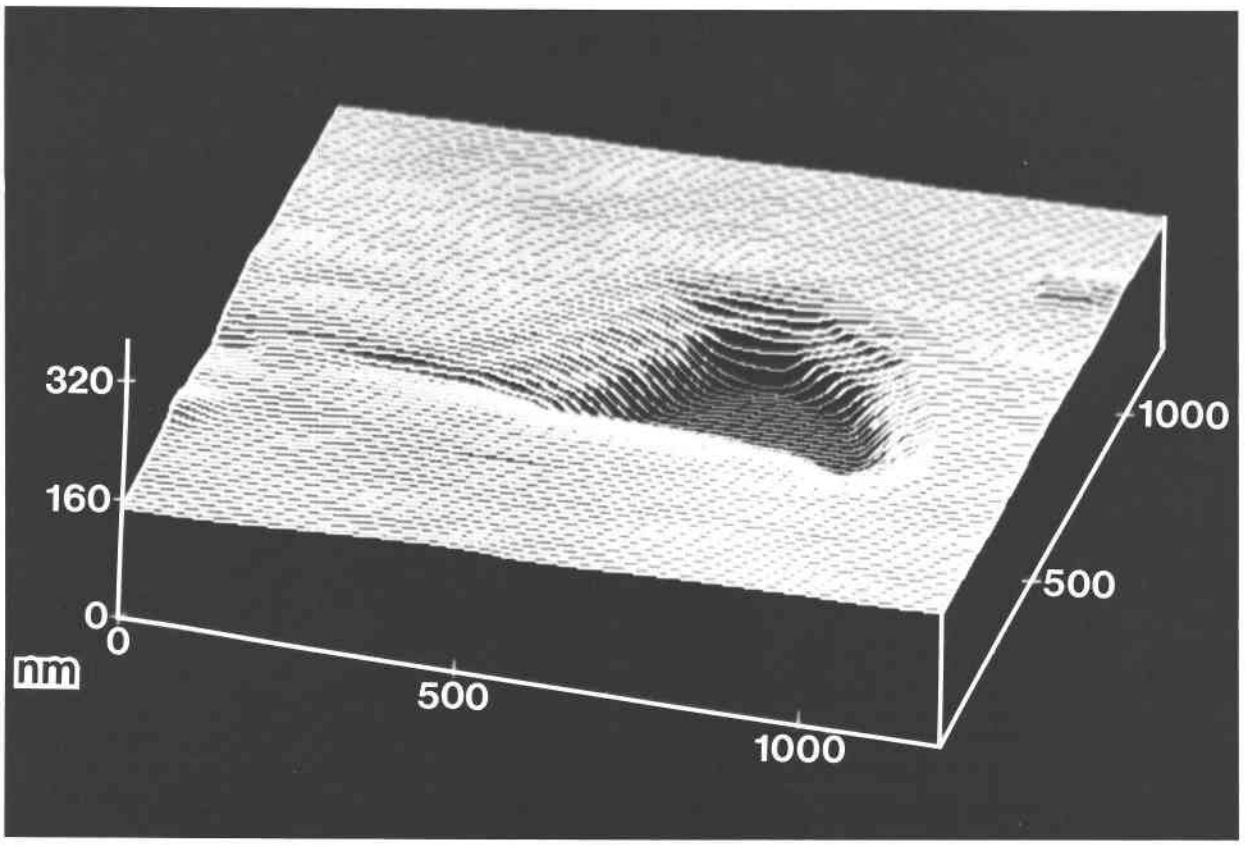

Fig. 3. AFM image of a pit 80 nm deep on an albite {010} cleavage surface. In this and all remaining figures, the axes are scaled in nanometers.

is derived from an even shallower depth because of the following. The reduced coordination shells of surface atoms are filled by atomic or molecular species sorbed from the air immediately after fracture (e.g., Hochella et al., 1986). This results in a monolayer or two of disordered adventitious species (e.g., O_2, H_2O, and CO_2) which only adds diffuse scattering to the LEED pattern background. However, the presence of the contaminant overlayer does mean that fewer monolayers of the albite surface contribute to the pattern, owing to electron attenuation by this overlayer. Therefore, probably only the top 2–4 monolayers of albite contribute to the LEED pattern, and the systematic absence due to the **c** centering halfway along **b** does not come into play.

The LEED results suggest that the albite {010} surface does not atomically reconstruct after exposure to air following fracture, but that there is a slight lateral relaxation of the surface atomic structure. Although we have not seen this previously in our study of the surface structures of hematite and calcite (Eggleston, Hochella, and Stipp, unpublished data), and it is not surprising or unexpected to see it for albite surfaces. Because of the low symmetry of this structure and the fact that surface atoms will seek equilibrium positions with the remainder of their original coordination shell before fracture, it might be expected that surface Na and O atoms (these reside on the albite {010} surface) and associated ligands will shift slightly, causing a slight change in the size and shape of the surface unit cell. Finally, relaxation perpendicular to the surface (in the form of a contraction typically in the range of several percent) is seen on many clean surfaces in a vacuum (Somorjai, 1981, and references therein). Although we do not have the data to measure relaxation in this direction, we would expect that this effect on the surface structure of albite would be relatively small and in the range of the lateral relaxation owing, at least in part, to surface bonding as a result of the adventitious overlayer.

AFM

Various AFM images of freshly fractured albite {010} surfaces are shown in Figures 3–6. Figure 3 shows a pit about 600 nm across and 80 nm deep, with a shallow (<20 nm) linear feature extending from one of its edges. Only very slight relief is apparent outside of the pit. A supposed void in an albite single crystal with a size and shape similar to this pit has been imaged with TEM by Eggleton and Buseck (1980). The TEM image even shows the same linear feature extending from the pit as seen in this AFM image. Eggleton and Buseck called these voids negative crystals because their boundaries parallel crys-

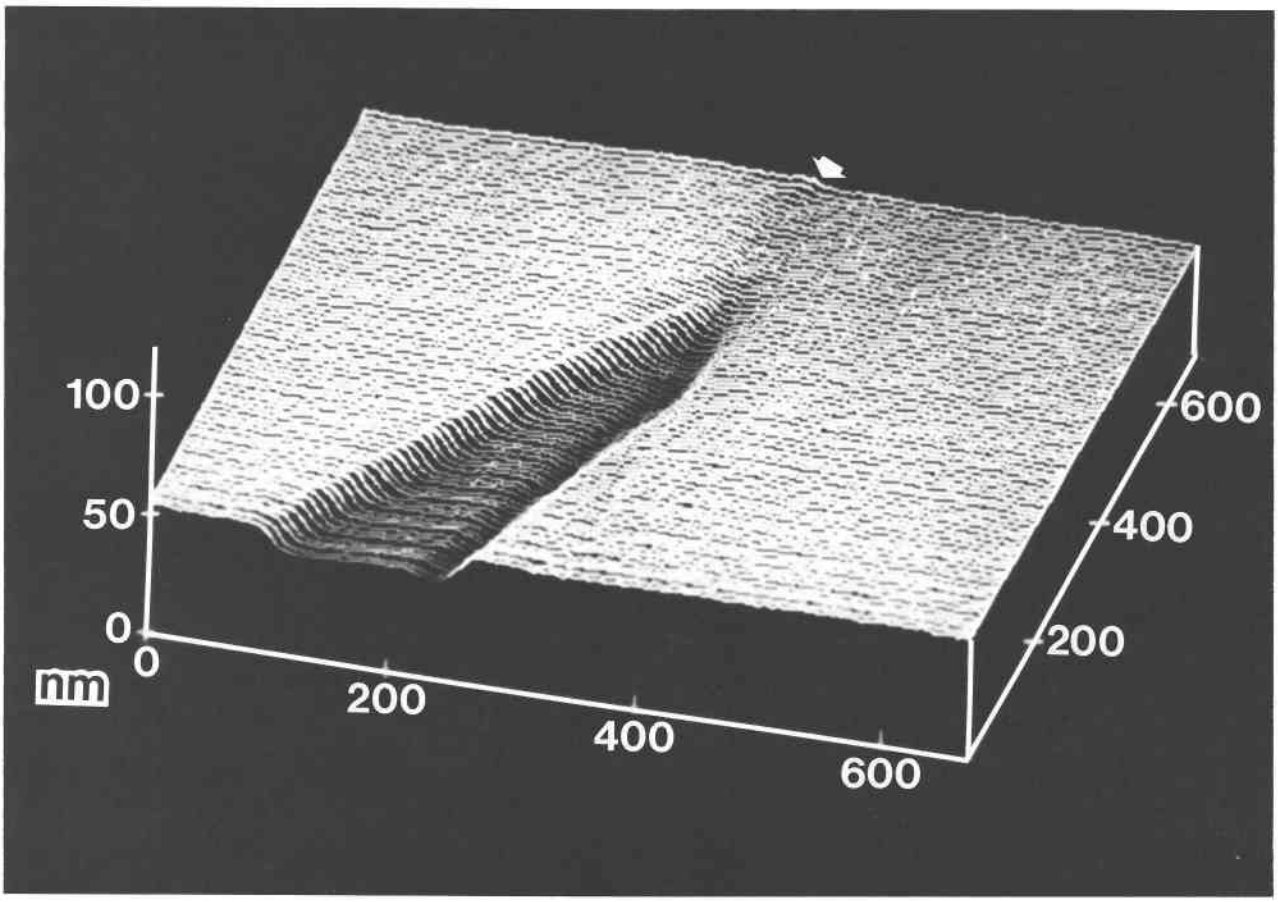

Fig. 4. AFM image of a wedge-shaped depression on the {010} surface of albite showing approximately 2:1 vertical exaggeration. The average depth of the feature is only 10 nm (100 Å). The left side of the wedge has a topographic expression that extends to the top of the image (marked by an arrow). The relief at the arrow is 4 nm.

tallographic directions. They also suspected that these features are due to mineral weathering, with fluids entering crystals along imperfections, crystal defects, and domain boundaries, resulting in internal dissolution. However, because the crystal we used showed no signs of external dissolution, the void that we have imaged may be a primary fluid inclusion. Whatever the cause of these features, the AFM image of this pit adds to the information obtainable from TEM by revealing the general shape of the inside of the pit, with stepped walls and a flat bottom. However, one might expect that the walls of this pit, including the apparent steps, are actually more blocky, i.e., with flat features, rather than the sloping walls that are shown in the image. In fact, the depth of the pit is roughly half the lateral extent of the pit walls from top to bottom. This same proportion is also observed for steps imaged in Figures 4 and 5, described below, indicating that the slope of the steps reflects the shape of the end of the tip interacting with the surface. Therefore, as the tip scans over a depression as shown in Figure 3, it is the side of the tip that interacts with the top edge of a step until the end of the tip reaches the bottom of the depression. At that point, the end of the tip again records the true surface shape until the opposite side of the tip contacts the opposite wall of the pit. Small features will be imaged closer to their true shape as the side of the tip interacting with a feature becomes more vertical. Nevertheless, the image in Figure 3 suggests that AFM will be very useful in following the incipient formation and growth of surface etch pits and related features in mineral dissolution experiments.

Figure 4 shows a curious wedge-shaped depression, which has an average depth of only 10 nm. This may also be an internal dissolution feature, as suggested for the pit described above, or it may be a fracture or inclusion feature. As described for Figure 3, the steepness of the steps that outline the depression is a function of the shape of the end of the diamond tip. As imaged, the lateral distance over the steps are approximately 20 nm, when in fact the steps are probably closer to vertical. In addition, if the steps imaged in Figure 4 are truly vertical, the tip must have a nearly symmetric shape, at least in the direction of the scan, because the steepness of the steps as imaged on both sides of the wedge is nearly the same.

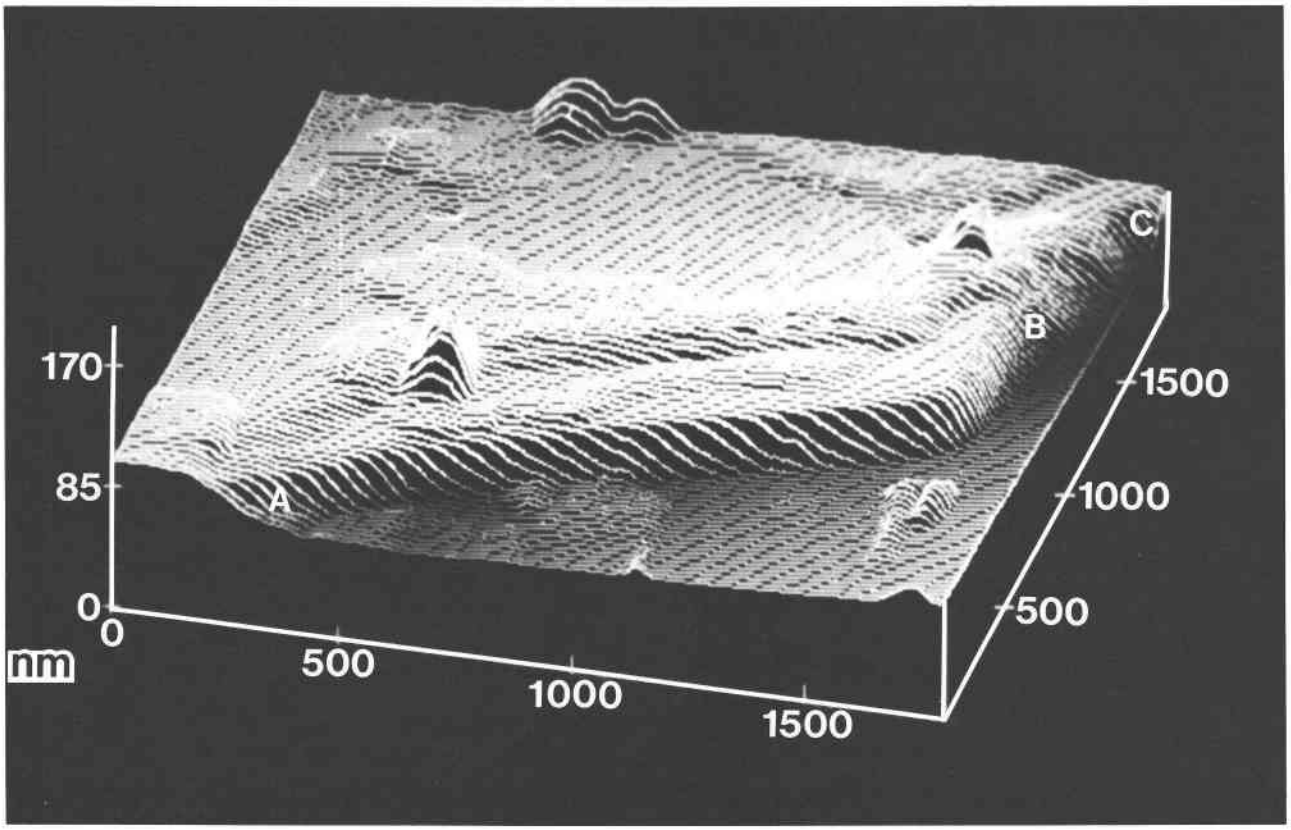

Fig. 5. AFM image of ultrafine particles (large bumps on the upper plateau) and a curving step 25 to 30 nm high on the {010} surface of albite. The vertical exaggeration is approximately 3:1. Between points A and B, the step appears to have a lateral extent of 60 nm. This is probably an artifact of the shape of the end of the tip. Between points B and C, the apparent lateral extent of the step increases to 150–200 nm, probably reflecting a true change in the step shape. See text for further explanation.

The left side of the wedge-shaped feature in Figure 4 appears to have a subtle topographic expression, in the form of a rise or step 2.5 to 4 nm high, extending beyond the tip of the wedge to the top of the image (the latter position has been marked by an arrow). The range in step height is not uncertainty in the measurement, but actual height differences that depend on exactly where the feature is measured. Besides the obvious steps defining the wedge-shaped depression and this slight rise off the tip of the wedge, the surface seems to be atomically flat.

Figure 5, with a vertical exaggeration of about 3:1, shows generally flat areas of the {010} albite surface with a few mounds (discussed below) separated by a curving step 25 to 30 nm high. The step between points A and B in the figure shows its maximum steepness with a lateral extent of approximately 60 nm from top to bottom. As before, this step may actually be vertical, and the lateral extent of the edge is probably a function of the shape of the tip. Between points B and C, the step is considerably wider in lateral extent (150 to 200 nm), reflecting a true change in step shape.

The mounds 20–40 nm high in Figure 5 remained in position while this area was imaged several times using different scan directions. However, after this sample was immersed in deionized water for 1 h and then air-dried, none of the mounds could be found with AFM. Therefore, we believe that these mounds may be ultrafine particles of albite resulting from fracture and held electrostatically to the surface. (Such particles are often called fracture dust.) The imaging of these ultrafine particles in Figure 5 clearly illustrates another important point about using AFM to provide high-resolution topographic images of surfaces. No matter how sharp the tip is, it cannot go under overhangs. A false image will be generated in these areas, as shown around the base of each particle.

Figure 6 is the highest resolution image presented in this study of the albite {010} surface. The field of view is 380 nm, and extremely small features can be seen. Cross sections through the image show a maximum apparent relief of 3 nm (around point A in the figure), although this must be considered a minimum value because of the tip shape. Most of the right half of the image appears to be atomically flat, with a measured relief of only 0.1–0.2 nm. The feature labeled B has a relief of 0.5 nm, whereas the area around point C consists of bumps 1 to 1.5 nm high. We attempted atomic resolution imaging over an

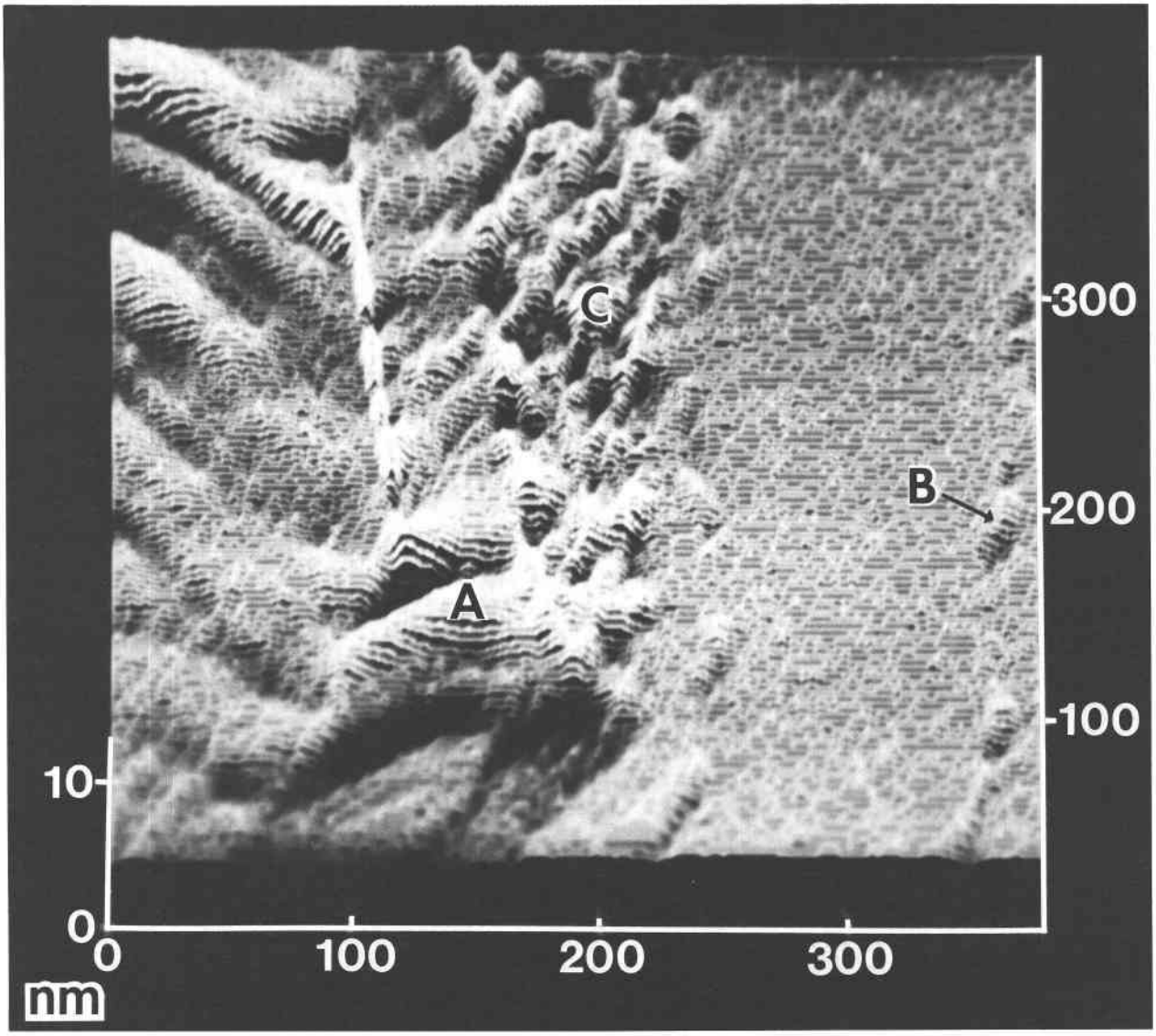

Fig. 6. High-resolution AFM image on the {010} albite surface tilted 60° toward the viewer. Most of the surface on the right side of the image is atomically flat, whereas the area on the left shows relief up to 3 nm around point A. The bump labeled B is only 0.5 nm (5 Å) high and 16 nm across. The relief around point C is 1 to 1.5 nm.

area 8 nm × 8 nm in the flat region, but we were not able to obtain an image showing atomic structure; these images did, however, confirm that this area is essentially atomically flat.

Conclusions

It is possible to gain insight into the atomic structure and very fine-scale morphology of insulating mineral surfaces with LEED and AFM. Using LEED, we have shown that the albite {010} surface, exposed by fracture in air at room temperature, exhibits slight lateral relaxation (i.e., distortion from the bulk structure), although the surface does not reconstruct. We envision this process as one in which surface atoms and associated ligands seek equilibrium positions in this low symmetry structure.

The morphology of the albite {010} cleavage surface can be quite variable, especially as seen with the extremely high spatial-resolution capability of the AFM, even though this surface is defined by well-developed cleavage. Fracture exposes extremely small internal dissolution features or voids formed during growth (Figs. 3 and 4), small cleavage steps (Fig. 5), and complex features like those shown in Figure 6. The surface morphology displayed in this latter figure is probably due to less than perfect crystallographic control of breakage. Fracture patterns of this sort have been observed for albite before with SEM, but at a much larger scale (unpublished data).

The techniques and procedures shown in this study and those of Hochella et al. (1989), Eggleston and Hochella (1990), and Hartman et al. (1990) could be used, for example, in the studies of mineral dissolution, sorption at the aqueous solution-mineral interface, and fracture propagation. For dissolution studies, AFM should allow researchers to observe directly and characterize the roles played by high energy sites, such as steps, kinks, pits, and defect outcrops, and it may allow for the observation of textural changes on mineral surfaces as leached layers develop. In sorption studies, LEED and AFM should be applicable in certain cases in determining the roles that surface atomic structure and morphology play in attachment processes. It also may be possible to use AFM to determine the spatial distribution of sorbed species. Finally, it is possible that AFM can be used to image the intersection of crack tips and surfaces at extremely high magnification; this may add to our knowledge of the effects of chemical environment and crack-tip morphology on crack propagation.

Atomic-force microscopy is still in its early stages of development. As shown in this study, AFM images are presently limited by the relatively crude tips that are used. With rigid and sharper tips coupled with smaller tracking forces, contact AFM images will improve considerably, and collecting atomic resolution images should become more routine.

Acknowledgments

We would like to thank the Center for Materials Research at Stanford University and Digital Instruments, Inc., for supporting this work. We are also grateful to George Parks, Gordon Brown, and Paul Ribbe for enlightening discussions. Thanks also to Don Peacor, Gary Sposito, and an anonymous reviewer who provided suggestions that improved the original manuscript.

References cited

Abraham, F.F., and Batra, I.P. (1989) Theoretical interpretation of atomic force microscope images of graphite. Surface Science, 209, L125–L132.

Albrecht, T.R., and Quate, C.F. (1987) Atomic resolution imaging of a nonconductor by atomic force microscopy. Journal of Applied Physics, 62, 2599–2602.

——— (1988) Atomic resolution with the atomic force microscope on conductors and nonconductors. Journal of Vacuum Science and Technology, 6, 271–274.

Alexander, S., Hellemans, L., Marti, O., Schneir, J., Elings, V., Hansma, P.K., Longmire, M., and Gurley, J. (1989) An atomic-resolution atomic-force microscope implemented using an optical lever. Journal of Applied Physics, 65, 164–167.

Binnig, G., and Smith, D.P.E. (1986) Single-tube three-dimensional scanner for scanning tunneling microscopy. Reviews of Scientific Instrumentation, 57, 1688–1689.

Binnig, G., Quate, C.F., and Gerber, Ch. (1986) Atomic force microscope. Physics Review Letters, 56, 930–933.

Binnig, G., Gerber, Ch., Stoll, E., Albrecht, T.R., and Quate, C.F. (1987) Atomic resolution with atomic force microscope. Surface Science, 189/190, 1–6.

Clarke, L.J. (1985) Surface crystallography, an introduction to low energy electron diffraction, 329 p. Wiley, New York.

Dawson, P.H. (1966) Secondary electron emission yields of some ceramics. Journal of Applied Physics, 37, 3644–3645.

Drake, B., Prater, C.B., Weisenhorn, A.L., Gould, S.A.C., Albrecht, T.R., Quate, C.F., Cannell, D.S., Hansma, H.G., and Hansma, P.K. (1989) Imaging crystals, polymers, and processes in water with the atomic force microscope. Science, 243, 1586–1589.

Eggleston, C.M., and Hochella, M.F., Jr. (1990) Scanning tunneling microscopy of sulfide surfaces. Geochimica et Cosmochimica Acta, 54, 1511–1517.

Eggleton, R.A., and Buseck, P.R. (1980) High resolution electron microscopy of feldspar weathering. Clays and Clay Minerals, 28, 173–178.

Hansma, P.K., Elings, V.B., Marti, O., and Bracker, C.E. (1988) Scanning tunneling microscopy and atomic force microscopy: Application to biology and technology. Science, 242, 209–216.

Hartman, H., Sposito, G., Yang, A., Manne, S., Gould, S.A.C., and Hansma, P.K. (1990) Molecular-scale imaging of clay mineral surfaces with the atomic force microscope. Clays and Clay Minerals, in press.

Heinzelmann, H., Meyer, E., Grutter, P., Hidber, H.-R., Rosenthaler, L., and Guntherodt, H.J. (1988) Atomic force microscopy: General aspects and application to insulators. Journal of Vacuum Science and Technology, 6, 275–278.

Henry, N.F.M., and Lonsdale, K., Eds. (1969) International tables for X-ray crystallography, vol. 1. Kynoch Press, Birmingham, England.

Hochella, M.F., Jr. (1988) Auger electron and X-ray photoelectron spectroscopies. In F.C. Hawthorne, Ed., Spectroscopic methods in mineralogy and geology. Mineralogical Society of America Reviews in Mineralogy, 18, 573–637.

Hochella, M.F., Jr., and Carim, A.F. (1988) A reassessment of electron escape depths in silicon and thermally grown silicon dioxide thin films. Surface Science, 197, L260–L268.

Hochella, M.F., Jr., Harris, D.W., and Turner, A.M. (1986) Scanning Auger microscopy as a high-resolution microprobe for geologic materials. American Mineralogist, 71, 1247–1257.

Hochella, M.F., Jr., Eggleston, C.M., Elings, V.B., Parks, G.A., Brown, G.E., Jr., Wu, C.M., and Kjoller, K. (1989) Mineralogy in two dimensions: Scanning tunneling microscopy of semiconducting minerals with implications for geochemical reactivity. American Mineralogist, 74, 1235–1248.

Marti, O., Drake, B., and Hansma, P.K. (1987) Atomic force microscopy of liquid-covered surfaces: Atomic resolution images. Applied Physics Letters, 51, 484–486.

Pool, R. (1990) The children of STM. Science, 247, 634–636.

Seah, M.P., and Dench, W.A. (1979) Quantitative electron spectroscopy of surfaces: A standard data base for electron inelastic mean free paths in solids. Surface and Interface Analysis, 1, 2–11.

Somorjai, G.A. (1981) Chemistry in two dimensions: Surfaces, 575 p. Cornell University Press, Ithaca, New York.

Van Hove, M.A., Weinberg W.H., and Chan, C.-M. (1986) Low-energy electron diffraction: Experiment, theory and surface structure determination, 603 p. Springer-Verlag, New York.

Weisenhorn, A.L., Hansma, P.K., Albrecht, T.R., and Quate C.F. (1989) Forces in atomic force microscopy in air and water. Applied Physics Letters, 54, 2651–2653.

Manuscript received February 5, 1990
Manuscript accepted May 20, 1990